Research Article

SOHAG JOURNAL OF SCIENCES

https://doi.org/ 10.21608/sjsci.2025.393488.1278

Tailoring Vanadium Oxide Thin Film Structure and Electrical Properties via Pulsed DC and RF Magnetron Sputtering

F. M. El-Hossary[1], A. M. Abd El-Rahman[2,1], Ali. A. El-kamle[1], Mohammed H. Fawey[1,*]

[1]*Physics Department, Faculty of Science, Sohag University, 82524 Sohag, Egypt*
[2]*King Abdulaziz University, Jeddah 21589, Kingdom of Saudi Arabia*
[*] *E-mail: mohammed.fawey@gmail.com*

Received: 16th June 2025 **Revised:** 18th August 2025 **Accepted:** 25th August 2025
Published online: 4th Septamper 2025

Abstract: Vanadium oxide thin films are increasingly explored for electronic, electrochemical, and energy-related applications due to their variable oxidation states and versatile physicochemical properties. This study systematically compares the effects of pulsed DC and RF magnetron sputtering techniques on the structural, morphological, and electrical characteristics of vanadium oxide films deposited on 304 AISI stainless steel substrates. High-purity vanadium target was sputtered in a controlled Ar/O_2 environment. X-ray diffraction (XRD) revealed that pulsed DC sputtering favored the formation of monoclinic VO_2, while RF sputtering promoted orthorhombic V_2O_5, indicating a phase transition driven by deposition parameters. The average crystallite size was smaller in pulsed DC films (~10.12 nm) than in RF films (~12.26 nm). X-ray photoelectron spectroscopy (XPS) showed that pulsed DC sputtering produced films with more stable V^{4+}/V^{5+} ratios and controlled stoichiometry. In contrast, RF-deposited films exhibited higher oxidation states and greater surface contamination due to porosity. Fourier transform infrared (FTIR) spectra confirmed these phase distinctions by identifying vibrational modes corresponding to VO_2-rich and V_2O_5-rich compositions. Scanning electron microscopy (SEM) revealed that pulsed DC film was thinner, denser, and smoother, while RF film was thicker with a porous nanostructure. Electrical measurements showed higher conductivity in pulsed DC films (~4.04×10^{-4} S/cm) than in RF films (~3.22×10^{-4} S/cm). These findings highlight the critical role of deposition technique in tailoring vanadium oxide thin films for advanced smart devices and energy systems.
Keywords: Vanadium oxide thin films; Pulsed DC magnetron sputtering; RF magnetron sputtering; FTIR; Electrical conductivity.

1. Introduction

In recent years, functional oxide materials exhibiting phase transitions have attracted growing interest from researchers due to their significance in a wide range of technological applications [1–3]. Among them, vanadium oxides (VO_x)—a family of transition-metal oxides—display various stoichiometries as a result of the multivalent nature of the vanadium cation. These include several sub-oxide phases such as V_2O_3, V_4O_9, V_6O_{13}, and the thermodynamically stable V_2O_5 phase, which is readily obtained under oxygen-rich conditions [4–6]. Owing to their tunable electrical conductivity, optical transparency, and semiconducting-to-metallic phase transitions [7], vanadium oxides are promising candidates for diverse applications. Their functional oxide phases have been utilized in devices such as gas sensors [8], electrical switches [9], thermochromic smart windows [10], thermal actuators [11], memory devices [12], photonic devices [13], tunable optical filters [14], optical switches [15], bolometers [16], and energy storage devices [17]. Achieving precise control over their structural, morphological, and physicochemical characteristics is therefore essential for optimizing performance in these applications.

A variety of synthesis routes have been employed to fabricate VO_x thin films, including hydrothermal synthesis [18], chemical vapor deposition (CVD) [19], pulsed laser deposition (PLD) [20], electron beam evaporation [21], sol–gel methods [22], and chemical solution processing [23]. Among these, magnetron sputtering stands out as an especially attractive technique due to its scalability, environmental friendliness (avoiding toxic solvents), and excellent reproducibility [24,25]. Direct current (DC) magnetron sputtering is a versatile physical vapor deposition (PVD) technique that allows fine control over film thickness, stoichiometry, crystallinity, and microstructure. Two widely adopted sputtering modes—pulsed direct current (pulsed DC) and radio frequency (RF)—offer distinct plasma characteristics, ion bombardment energies, and growth kinetics, which can result in notable differences in film formation. Pulsed DC sputtering minimizes target arcing and enhances deposition rates when working with partially insulating oxide targets, whereas RF sputtering is particularly well-suited for insulating or semi-insulating materials because it can process non-conductive targets [26]. Furthermore, RF sputtering typically operates at lower substrate temperatures, enabling high-quality film deposition on a variety of substrates without causing thermal damage. Films deposited by RF sputtering often exhibit excellent uniformity, adhesion, and compositional control. By adjusting parameters such as power, pressure, and gas composition, RF sputtering can produce films with tailored structural and electrical characteristics. However, direct comparisons of VO_x thin films deposited by pulsed DC and RF magnetron sputtering under identical reactive conditions are

scarce. Most existing studies either focus on a single deposition mode or vary multiple parameters simultaneously, making it challenging to isolate the intrinsic influence of sputtering mode on film growth mechanisms and resulting properties. This gap in the literature limits our understanding of how deposition mode alone governs phase evolution, grain structure, surface morphology, and electrical behavior.

In this work, nanostructured vanadium oxide thin films were deposited onto 304 AISI stainless steel substrates using both pulsed DC and RF magnetron sputtering under identical reactive gas composition, working pressure, target–substrate distance, and substrate conditions. This controlled approach isolates the role of sputtering mode in determining the structural, morphological, and electrical characteristics of the films. The findings provide clear insights into the deposition–structure–property relationship, offering valuable guidelines for tailoring vanadium oxide thin films in functional materials applications where precise control over morphology and electrical properties is crucial, such as advanced electronic devices, optical systems, and energy storage technologies.

2. Materials and methods

In this study, vanadium oxide thin films were deposited onto 304 stainless steel substrates using both pulsed DC and RF magnetron sputtering systems. A schematic representation of the sputtering apparatus is provided in Fig. (1). A 304 AISI stainless steel sheet with a thickness of 1 mm was sectioned into 10 × 10 mm samples. Prior to deposition, the substrates underwent ultrasonic cleaning in ethanol for 10 minutes using an ultrasonic cleaner (Struers Metason 120 T) to remove surface contaminants. A high-purity vanadium target (99.99%), with a diameter of 50.8 mm and a thickness of 3 mm, served as the source material. The deposition was conducted in a reactive environment composed of Ar and O_2. Prior to initiating the sputtering process, regardless of whether pulsed DC or RF power was applied, the target-to-substrate distance was precisely set to 7 cm. The vacuum chamber was initially evacuated using a dual-stage rotary pump coupled with a turbomolecular pump, reaching a base pressure of 5×10^{-5} mbar within approximately two hours. Once the desired vacuum level was attained, a reactive gas mixture containing 5% O_2 and 95% Ar was introduced to establish a working pressure of approximately 9.5×10^{-3} mbar. After pressure stabilization within the chamber, the appropriate power source—either pulsed DC or RF—was employed to initiate the sputtering of the vanadium target. For pulsed DC magnetron sputtering, a pulsed DC power supply (Advanced Energy Pinnacle Plus) was utilized. The system operated at a power level of 250 W, with a pulse frequency of 150 kHz and an off-time of 2 µs per cycle. The deposition process was maintained for a total of 150 minutes, resulting in a final thickness of about 350 nm. In contrast, the RF magnetron sputtering process used an RF power generator (ENI OEM-12A) configured to deliver 250 W of power. The process was conducted for 50 minutes, yielding a vanadium oxide film with a thickness of approximately 400 nm. Real-time monitoring of deposition rate and film thickness is achieved using an integrated thickness sensor (Inficon SQM-160). In addition, the final film thickness was verified after deposition using a Form Talysurf Intra profilometer (Form Talysurf 50). Profilometry was chosen over cross-sectional SEM as it offers higher accuracy for smooth films and is non-destructive. This approach confirmed the measured thickness values and validated the deposition rate differences between pulsed DC and RF sputtering. To promote uniform film deposition, the substrate holder was continuously rotated, completing a full 360˚ revolution every 15 seconds, alternating between clockwise and counterclockwise directions. This motion is governed by a programmable oscillation controller (Model: DCS-GP-SMC-2K12), which enables fine-tuned regulation of both rotational speed and direction. To prevent overheating and ensure thermal stability throughout the sputtering process, the targets are actively cooled via an industrial chiller system (Model: CW-5200), which maintains the coolant at a stable temperature of 10 ˚C. Upon completion of the sputtering process, the samples were allowed to cool within the vacuum chamber for 30 minutes prior to exposure to atmospheric conditions.

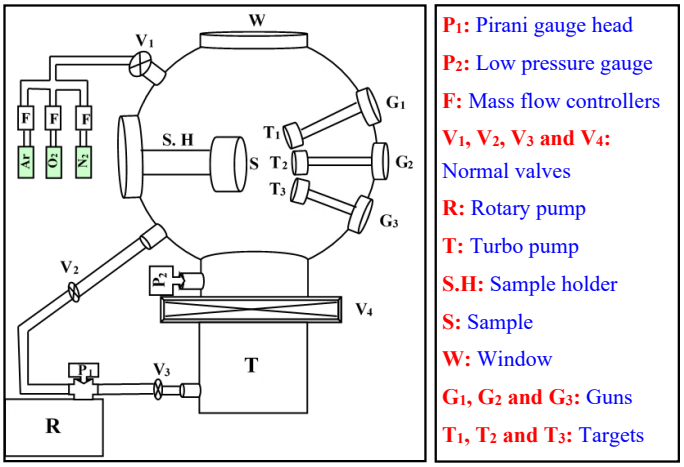

Fig. 1: Schematic diagram of the pulsed DC and RF magnetron sputtering system

Post-deposition, the thin films underwent a comprehensive set of characterization procedures to assess their structural and morphological attributes. Structural evaluation was performed using X-ray diffraction (XRD) on a Bruker D8 ADVANCED diffractometer, utilizing Cu Kα radiation (λ = 1.5406 Å). Data acquisition was conducted at a scan rate of 2˚/min with a step size of 0.02˚, spanning a 2θ range from 20˚ to 80˚, ensuring accurate identification of crystal phases and lattice configurations. Surface morphology and topographical features of the vanadium oxide thin films were investigated using field emission scanning electron microscopy (FE-SEM) and conventional SEM, employing FEI Quanta FEG 250 and Sigma 500 VP instruments, respectively. These techniques provided high-resolution insights into grain size, surface texture, and microstructural variations influenced by the sputtering method. Both images were captured at a consistent magnification of 15,000x, but under different accelerating voltages (5 kV and 30 kV), reflecting the operational conditions of the two SEM systems used. This setup enabled the visualization of fine surface details while preserving the inherent imaging characteristics of each instrument. To further investigate the chemical composition and bonding characteristics of the

vanadium oxide layers, Fourier Transform Infrared (FTIR) spectroscopy was performed using an Alpha Bruker Platinum ATR spectrometer. Measurements were obtained in attenuated total reflection (ATR) mode, with spectral output reported in wavenumbers (cm^{-1}). Spectra were collected within the 2500–400 cm^{-1} range, at a resolution of 4 cm^{-1}, with each spectrum representing the average of 32 scans to enhance signal clarity and ensure accurate identification of vibrational modes. X-ray photoelectron spectroscopy (XPS) analyses were conducted using a K-ALPHA spectrometer (Thermo Fisher Scientific, USA) equipped with a monochromated Al Kα radiation source (photon energy = 1486.6 eV). Spectral data were collected across a binding energy range of -10 to 1350 eV using a 400 µm spot size and an electron take-off angle of 90˚. The analysis chamber was maintained at an ultra-high vacuum with a base pressure below 6×10^{-9} mbar. Survey scans were acquired at a pass energy of 200 eV, while high-resolution spectra were recorded at 50 eV. No Ar^+ ion sputtering was performed to preserve the native chemical composition of the sample surfaces. All binding energies were calibrated against the C 1s reference peak at 284.8 eV. To minimize contamination, all samples were stored in a clean, controlled incubator with stable temperature and humidity, sealed in individual containers, and handled exclusively with clean gloves and tools. Electrical characterization of the vanadium oxide thin films was carried out using a CORRTEST Instruments Bipotentiostat/Galvanostat (Model CS2350M, China). Electrical conductivity was measured via the potentiodynamic technique, employing a linear voltage sweep ranging from –0.01 V to 0.1 V relative to the open-circuit potential (OCP) at a scan rate of 0.5 mV/s. To eliminate any influence from the conductive stainless-steel substrate, electrical conductivity was measured using a clip-based configuration in which the current flows laterally through the thin film, with the film positioned between the two clip contacts. All measurements were conducted under identical ambient conditions to guarantee experimental consistency and ensure the reproducibility of results.

3. Results and Discussion:

3.1. X-ray analysis:

The XRD patterns of vanadium oxide thin films deposited via pulsed DC magnetron sputtering and RF magnetron sputtering, as shown in Fig. (2), exhibit distinct differences in phase composition and crystallinity. These differences indicate a structural transition from predominantly monoclinic VO_2 in DC-sputtered film to largely orthorhombic V_2O_5 in RF-sputtered film. Phase identification is consistent with ICSD reference data for VO_2 [ICSD: 80928] and V_2O_5 [ICSD: 653926]. The monoclinic VO_2 phase is defined by a = 12.0536 Å, b = 3.6938 Å, c = 6.4217 Å, and β = 106.9250˚, whereas the orthorhombic V_2O_5 phase is characterized by lattice parameters a = 11.519 Å, b = 4.373 Å, and c = 3.564 Å. Table (1) summarizes selected 2θ values, Miller indices (hkl), and corresponding phases, confirming the presence of both VO_2 and V_2O_5 in mixed-phase regions for both sputtering techniques.

The observed phase transition from VO_2 to V_2O_5 is primarily attributed to variations in deposition parameters, such as plasma energy distribution, and sputtering power. In pulsed DC-sputtered film, the XRD patterns are dominated by monoclinic VO_2 reflections corresponding to the (003), $(\bar{5}\bar{1}1)$, $(\bar{3}13)$, and (203) planes at 44.1˚, 44.85˚, 50.75˚, and 51.2˚, respectively. These peaks partially overlap with reflections corresponding to orthorhombic V_2O_5, namely the (220), (510), (002), and (221) planes, suggesting the presence of a mixed-phase region. The preferential formation of VO_2 is linked to the higher ion bombardment energy inherent in pulsed DC systems, which promotes the stabilization of intermediate oxidation states (V^{4+}) [24,27]. The limited presence of V_2O_5 peaks under these conditions suggests a suppressed oxidation environment, possibly due to reduced oxygen incorporation or partial reduction of V_2O_5 to VO_2 caused by energetic particle interactions [28]. In contrast, RF-sputtered film displays a set of orthorhombic V_2O_5 reflections, including prominent peaks from the (220), (331), and (612) planes at 44.1˚, 74.85˚, and 75.5˚, respectively. This enhanced phase complexity and crystallinity are indicative of more complete oxidation processes. The uniform energy distribution and higher plasma density typical of RF sputtering favor the formation of fully oxidized V^{5+} states, stabilizing the V_2O_5 phase [29,30]. The coexistence of multiple V_2O_5 peaks in RF-deposited film aligns with its ability to sustain reactive oxygen species (e.g., O^- ions), which promote complete oxidation and structural diversification [27,28]. Additionally, the lower electron temperature in RF sputtering facilitate controlled oxidation via extended interaction with oxygen radicals [27,30]. In contrast, the intermittent, high-energy ion bombardment in pulsed DC sputtering may induce localized heating and favor the formation of metastable VO_2 over the thermodynamically stable V_2O_5 phase [24,31].

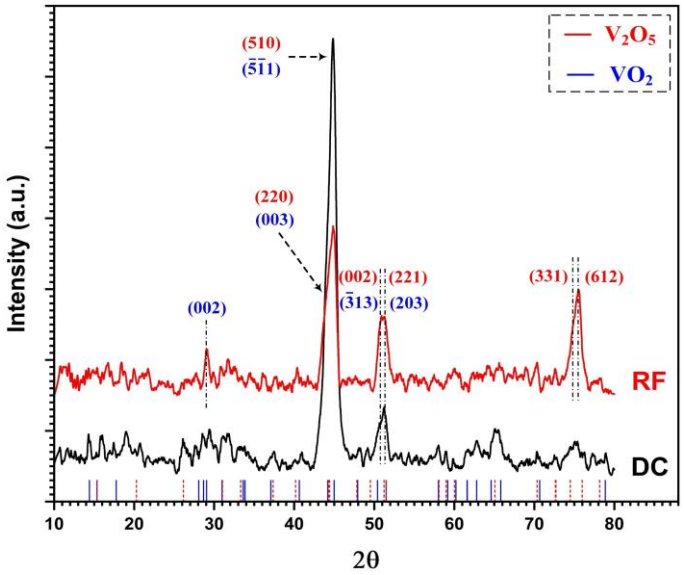

Fig. 2: XRD patterns of vanadium oxide thin films deposited using pulsed DC magnetron sputtering and RF magnetron sputtering. Reference diffraction lines from ICSD cards for VO_2 (blue) and V_2O_5 (red) are shown below the patterns.

From a thermodynamic perspective, vanadium oxide phase stability is strongly dependent on oxygen partial pressure. The Gibbs free energy of formation (ΔG^f) for VO_2 is favored under moderately reduced oxygen environments, whereas V_2O_5 is stabilized under oxygen-rich conditions due to its lower ΔG^f at higher oxygen chemical potentials. In pulsed DC sputtering,

energetic ion bombardment reduces the effective oxygen activity at the growth front, shifting the equilibrium toward VO_2. By contrast, the lower ion energies and higher oxygen partial pressure in RF sputtering thermodynamically stabilize the V^{5+} state, favoring V_2O_5 formation. Collectively, the interplay between plasma–substrate interactions and thermodynamic driving forces explains the predominance of VO_2 in pulsed DC films and V_2O_5 in RF films.

Table 1: XRD results for selected diffraction peaks, including 2θ values, Miller indices (hkl), and the corresponding crystalline phases

	2θ	hkl (VO_2)	hkl (V_2O_5)
DC	44.1	(003)	(220)
	44.85	$(\bar{5}\bar{1}1)$	(510)
	50.75	$(\bar{3}13)$	(002)
	51.2	(203)	(221)
RF	29.1	(002)	--
	44.1	(003)	(220)
	44.8	$(\bar{5}\bar{1}1)$	(510)
	50.8	$(\bar{3}13)$	(002)
	51.2	(203)	(221)
	74.85	--	(331)
	75.5	--	(612)

Crystallite sizes of the thin films were estimated using the Scherrer equation ([32],

$$D = \frac{K\lambda}{\beta \cos\theta} \quad (1)$$

where D is the average crystallite size, K is the shape factor (typically 0.9), λ is the X-ray wavelength, β is the full width at half maximum (FWHM) of the diffraction peak, and θ is the diffraction angle (Bragg angle). The calculated crystallite sizes are presented in Table (2). A multi-peak fitting procedure, considering both dominant and minor diffraction reflections, was used to evaluate average crystallite size, providing a more precise and statistically reliable estimate than the traditional single-peak method. The film deposited via pulsed DC magnetron sputtering exhibited an average crystallite size of ~10.12 nm, whereas the RF-sputtered counterpart demonstrated a slightly larger size of ~12.26 nm. This variation is primarily attributed to the distinct plasma characteristics and ion bombardment energies inherent to each sputtering technique. Pulsed DC sputtering generates higher energy ions via its unidirectional pulsed field, enhancing adatom mobility and inducing frequent re-nucleation events that disrupt grain growth, leading to finer grains and denser films [33,34]. In contrast, RF sputtering's alternating electric field and lower ion energy enable greater adatom diffusion, resulting in fewer nucleation events, larger crystallite formation, and increased porosity. The crystallite sizes reported in the present work are notably smaller than those observed in a prior study by Margoni et al. [35], who synthesized vanadium pentoxide (V_2O_5) thin films using spray pyrolysis. Their method employed an aqueous solution of ammonium metavanadate, supplemented with nitric acid, and deposition was conducted at substrate temperatures ranging from 300 ˚C to 400 ˚C. In their findings, crystallite size increased from 24.2 nm at 300 ˚C to a peak of 42.3 nm at 375 ˚C, followed by a reduction to 21 nm at 400 ˚C. The decrease at higher temperature was attributed to partial amorphization or increased structural disorder resulting from excessive thermal input.

The nanocrystalline structure and phase coexistence observed in both film types underscore the thermodynamic instability of vanadium oxide systems and highlight the strong dependence of structural characteristics on deposition technique. These structural differences bear significant implications for application. VO_2, favored by pulsed DC sputtering, undergoes a metal-insulator transition (MIT) near room temperature, making it highly promising for thermochromic coatings and electronic switching applications due to its reversible changes in electrical and optical properties [36]. In contrast, V_2O_5, which is predominantly formed in RF-sputtered film, exhibits a wider bandgap and high surface reactivity, rendering it suitable for electrochemical and catalytic applications such as LIBs and gas sensors [37,38]. The coexistence of VO_2 and V_2O_5 phases, in combination with nanoscale crystallite dimensions, may impart multifunctional properties to the films, enhancing surface activity and device performance. Consequently, the chosen sputtering method critically influences the crystalline phase composition, microstructure, and functional potential of vanadium oxide thin films. Moreover, tailoring deposition parameters—including power, oxygen flow rate, substrate temperature, and chamber pressure—is therefore essential for optimizing these materials for specific technological applications [39,40].

Table 2: Average crystallite size (nm) of vanadium oxide thin films deposited using pulsed DC magnetron sputtering and RF magnetron sputtering.

	2θ	FWHM	Crystallite Size (nm)	Average crystallite size (nm)
DC	44.1	1.1567	7.41	10.12 ± 1.38
	44.85	0.9164	9.38	
	50.75	0.9045	9.72	
	51.2	0.6314	13.95	
RF	29.1	0.4889	16.79	12.26 ± 1.65
	44.1	1.2191	7.03	
	44.8	0.7058	12.17	
	50.8	0.5685	15.47	
	51.2	0.9448	9.32	
	74.85	1.3072	7.65	
	75.5	0.5776	17.40	

3.2 Scanning electron microscopy:

SEM was employed to investigate the surface morphology of vanadium oxide thin films deposited via pulsed DC magnetron sputtering and RF magnetron sputtering. As shown in Fig. (3), the SEM images reveal distinct morphological differences between the two film types, underscoring the critical

influence of deposition technique on film microstructure. These variations are primarily attributed to differences in energy transfer mechanisms, plasma characteristics, and ion bombardment dynamics inherent to each sputtering method.

Thin film deposited using pulsed DC magnetron sputtering exhibits dense surfaces with a uniform and compact grain structure. The average film thickness is approximately 350 nm. This morphology reflects good continuity, low porosity, and relatively larger grains with well-defined boundaries, indicative of partial crystallinity and preferential growth orientation. The enhanced surface rearrangement and minimized void formation, driven by higher-energy ion bombardment, contribute to the formation of dense microstructures [41]. Such characteristics, often associated with limited adatom mobility and reduced thermal energy input, also confer improved mechanical stability and adhesion [42,43]. These features are especially advantageous for LIB cathodes, where long-term cycling stability and mechanical robustness are essential. Additionally, the pulsed DC-sputtered film exhibits a characteristic blue coloration, often associated with sub-stoichiometric vanadium oxides (e.g., VO_2 or mixed-valence V^{4+}/V^{5+} phases). This suggests the preferential formation of oxygen-deficient phases under the pulsed DC regime, likely due to reduced oxygen partial pressure during deposition, as supported by the XPS analysis (Section 3.3).

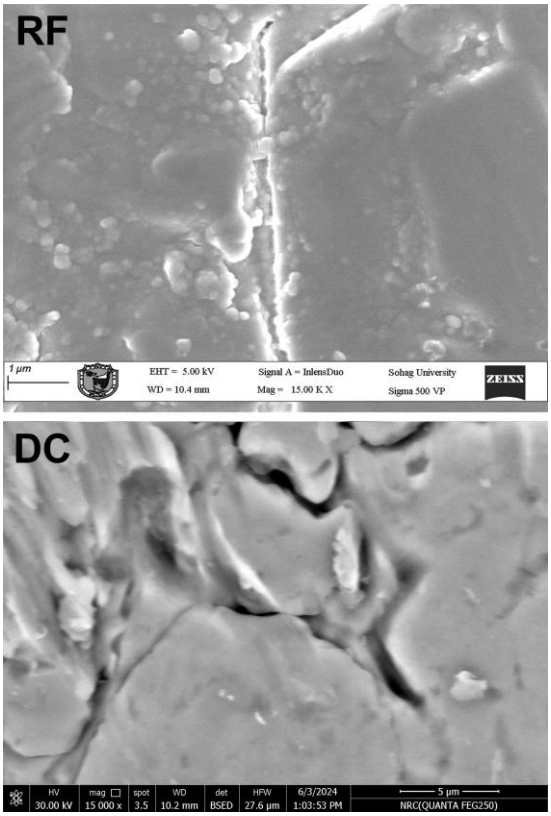

Fig. 3: SEM images of vanadium oxide thin films deposited using pulsed DC magnetron sputtering and RF magnetron sputtering.

In contrast, film deposited via RF magnetron sputtering is notably thicker (~400 nm) and exhibit a porous nanostructure with rougher surface features. This morphology is characterized by finer grains and a higher surface area, which is better for enhancing electrochemical activity. It should be noted that the comparison of grain size between films deposited by pulsed DC and RF magnetron sputtering is qualitative and based solely on visual inspection of the SEM images, without quantitative measurement. The increased thickness observed in RF-sputtered film, relative to those deposited via pulsed DC sputtering, is attributed to the differences in plasma behavior and power delivery. RF sputtering operates at a continuous alternating frequency (13.56 MHz), sustaining a denser plasma with higher ionization efficiency, thereby resulting in a higher sputtering yield and deposition rate. In contrast, pulsed DC sputtering involves periodic power interruptions to suppress arcing and mitigate target poisoning, especially relevant when working with oxide targets. These interruptions inherently reduce the net power delivered to the plasma, resulting in a lower overall deposition rate. Moreover, RF sputtering offers notable advantages, including compatibility with insulating targets and reduced susceptibility to target poisoning, which contribute to enhanced material removal efficiency. As a result, for equivalent deposition durations, RF sputtering generally yields thicker films. In contrast, pulsed DC sputtering tends to produce thinner, denser, and more uniform coatings due to its more controlled and energetic film growth kinetics. The increased porosity observed in films produced by RF sputtering is primarily attributed to fundamental differences in plasma characteristics and growth mechanisms between the two techniques. Specifically, RF sputtering generates lower ion bombardment energy at the substrate surface, which limits the surface mobility of adatoms during film growth. This insufficient energy prevents the atoms from diffusing into more stable, densely packed positions, leading to the development of a more porous microstructure. Furthermore, RF plasmas generally exhibit higher impedance compared to pulsed DC plasmas, which limits the ion flux and reduces the average ion energy reaching the substrate. Consequently, the level of energetic bombardment required to compact and densify the growing film is less effective in RF sputtering, further contributing to the development of a porous morphology. Such features provide larger surface areas and shorter ion diffusion paths, both of which are beneficial for improving the electrochemical reactivity of LIB cathodes. Furthermore, the yellow coloration observed in RF-sputtered film indicates the predominance of stoichiometric V_2O_5, characterized by a dominant V^{5+} oxidation state. This points to more complete oxidation during film growth, facilitated by RF sputtering's higher plasma density and efficient energy transfer. The resulting V_2O_5-rich film not only exhibits improved crystallinity but also offers superior charge-transfer kinetics and electrochemical performance [44].

Overall, the morphological, structural, and optical differences between pulsed DC- and RF-sputtered films demonstrate that the choice of sputtering technique strongly governs the composition and properties of vanadium oxide thin films. Pulsed DC sputtering produces dense, smooth films that are well suited for mechanically stable, long-cycling LIB cathodes, whereas RF sputtering yields thicker, porous, and more reactive films that are advantageous for applications requiring high electrochemical performance. Thus, careful optimization of the deposition method is critical for tailoring vanadium oxide thin films to specific functional requirements.

3.3 XPS analysis:

XPS was employed to examine the influence of deposition technique on the surface chemistry, oxidation states, and stoichiometry of vanadium oxide thin films fabricated via pulsed DC magnetron sputtering and RF magnetron sputtering. High-resolution spectra of the V 2p, O 1s, and C 1s core levels revealed significant variations in both binding energies and atomic concentrations depending on the sputtering method used. Figures (4) and (5) present the XPS survey and high-resolution spectra for the V 2p, O 1s, and C 1s regions of films deposited by pulsed DC and RF magnetron sputtering, respectively. The survey spectra for both techniques confirm the presence of the primary constituent elements—vanadium, oxygen, and carbon—which are clearly identified. Additionally, minor peaks were observed, likely originating from substrate-related impurities or adventitious contamination introduced during sample handling. These secondary features do not interfere with the core-level regions of interest and therefore do not influence the chemical state analysis. As such, the discussion focuses on the main elements, with particular attention to carbon as an indicator of surface contamination resulting from brief atmospheric exposure during sample transfer. Table (3) summarizes the binding energies (eV) and corresponding atomic percentages of the V 2p, O 1s, and C 1s core-level components in vanadium oxide thin films produced by both deposition methods. A comparative analysis reveals significant differences between films produced by pulsed DC and RF sputtering, reflecting the influence of plasma characteristics and energy input inherent to each method.

In terms of vanadium oxidation states, both techniques yield films containing mixed-valent vanadium species (V^{4+} and V^{5+}), characteristic of sub-stoichiometric vanadium oxides or amorphous phases [45]. The pulsed DC-sputtered film shows a more balanced distribution, with approximately 60.8% V^{5+} and 39.2% V^{4+}, suggesting a moderately oxidized film consistent with a near-stoichiometric V_2O_5 matrix that includes some VO_2 phase. In contrast, the RF-deposited film contains over 69% V^{5+}, indicating a stronger tendency toward V_2O_5 formation [46]. Analysis of the relative contributions of V^{4+} (V $2p_{3/2}$ + V $2p_{1/2}$) and V^{5+} (V $2p_{3/2}$ + V $2p_{1/2}$) oxidation states yields estimated VO_2/V_2O_5 ratios of 64.42% for the pulsed DC film and 44.84% for the RF film. These findings are consistent with the XRD results, which reveal additional diffraction peaks corresponding to the orthorhombic V_2O_5 phase in the RF-sputtered film. Furthermore, a notable shift in the V 2p binding energies toward higher values in the RF film may reflect stronger interactions between vanadium and surface hydroxyl or carbon-oxygen groups, or may arise from charging effects linked to the film's increased porosity or defect density [46]. The lower V^{4+} contribution in RF-sputtered film suggests enhanced oxidation, albeit at the expense of stoichiometric precision.

The O 1s spectra further support these trends. Multiple components are present, corresponding to distinct oxygen environments within the films. The primary peak at 530.1–530.3 eV is attributed to lattice oxygen (O^{2-}) in vanadium–oxygen frameworks, typical of VO_2 and V_2O_5 phases [30,47]. In pulsed DC-sputtered film, this lattice oxygen peak (~530.34 eV) constitutes more than half the total oxygen signal, with the remainder attributed to surface hydroxyl groups (OH^-) from adsorbed moisture [48]. This high lattice oxygen content indicates a well-oxidized, chemically stable matrix. Conversely, the RF-deposited film exhibits a dramatically reduced lattice oxygen fraction (only 8.2%), along with a dominant contribution from hydroxyl groups (36%) and a strong signal at 533.69 eV from oxygenated carbon species (C–O/C=O), absent in the DC film. These features suggest substantial surface adsorption of moisture or carbonaceous compounds, likely due to a more porous surface. The presence of this peak is consistent with literature reports that airborne organic molecules and water readily adsorb on oxide surfaces with high surface energy or structural disorder [48]. These observations are corroborated by SEM analysis, which reveals a porous nanostructure with rough surface morphology in the RF film.

Table.3: Binding energies (eV) and atomic percentages (%) of the V 2p, O 1s, and C 1s core-level components in vanadium oxide thin films deposited by pulsed DC and RF magnetron sputtering.

	Binding energy (eV)		Atomic percentage (%)	
	DC	RF	DC	RF
V $2p_{3/2}$ (V^{4+})	515.07	514.87	22.24	29.57
V $2p_{3/2}$ (V^{5+})	516.5	518.02	53.45	40.2
V $2p_{1/2}$ (V^{5+})	522.55	523.7	7.37	28.84
V $2p_{1/2}$ (V^{4+})	524	525.78	16.94	1.39
O 1s (V-O)	530.34	530.25	52.42	8.23
O 1s (OH)	531.4	532.11	47.58	35.97
O 1s (C-O/C=O)	--	533.69	--	55.8
C 1s (C-C/C-H)	284.77	284.86	75.28	66.65
C 1s (C-O/C-OH)	286.04	286.26	4.98	22.33
C 1s (O-C=O)	288.72	288.62	19.74	11.02

Despite precautions to limit contamination, the C 1s spectra show the presence of surface carbon, primarily attributed to ambient exposure during sample handling and transfer. A dominant peak at ~284.8 eV corresponds to C–C and C–H bonds typical of adventitious carbon [49,50]. Such contamination is routinely observed in XPS and does not significantly affect the interpretation of vanadium oxidation states [51]. However, carbon speciation reveals differences in surface chemistry: the pulsed DC film is dominated by hydrocarbon species (C–C/C–H), while the RF film exhibits a higher proportion of oxidized carbon groups (C–O, O–C=O) [49,50], reflecting stronger surface interactions with atmospheric carbon-containing species. This aligns with the increased hydroxyl and oxygenated content in the RF film, suggesting greater surface reactivity or moisture retention. Given that all samples were subjected to identical handling and storage conditions after deposition, the higher carbon content and contamination observed in RF-sputtered films can therefore be attributed to intrinsic surface chemistry associated with the deposition process rather than to environmental exposure.

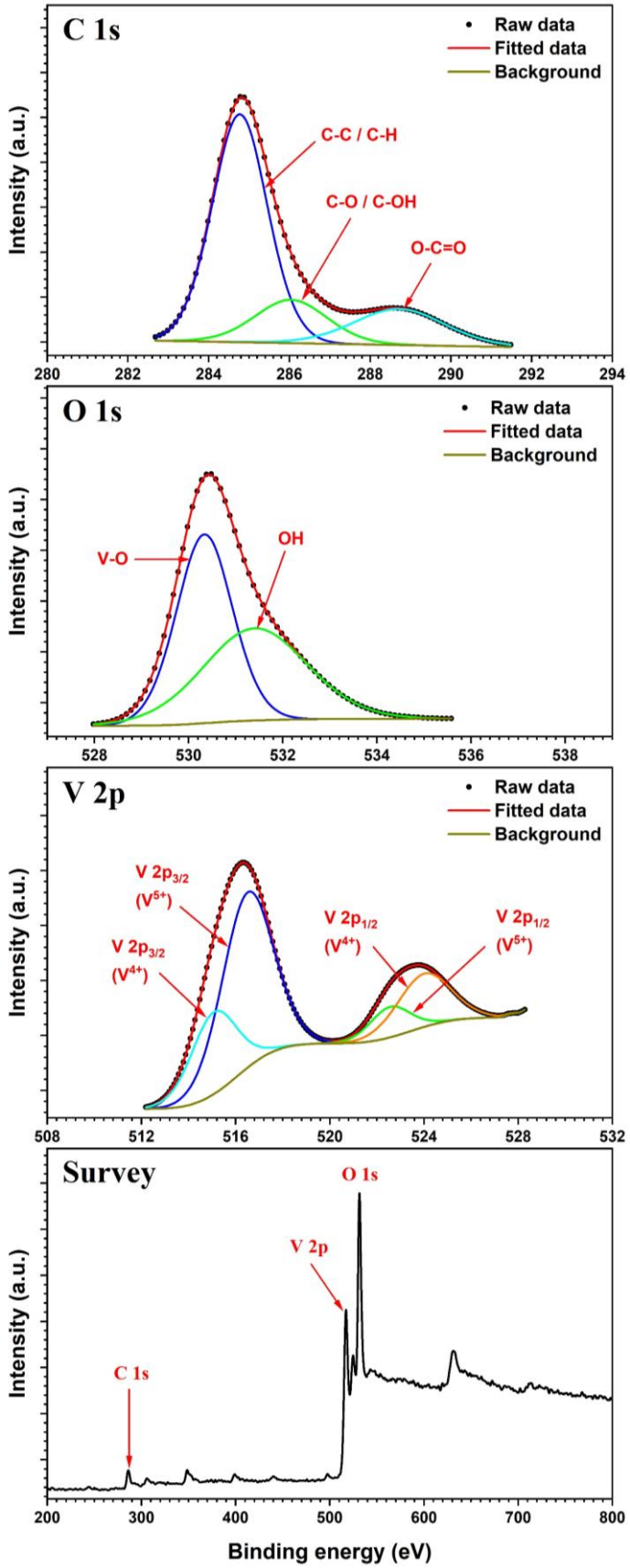

Fig .4: XPS survey and high-resolution spectra of the V 2p, O 1s, and C 1s core levels for vanadium oxide thin films deposited by Pulsed DC magnetron sputtering.

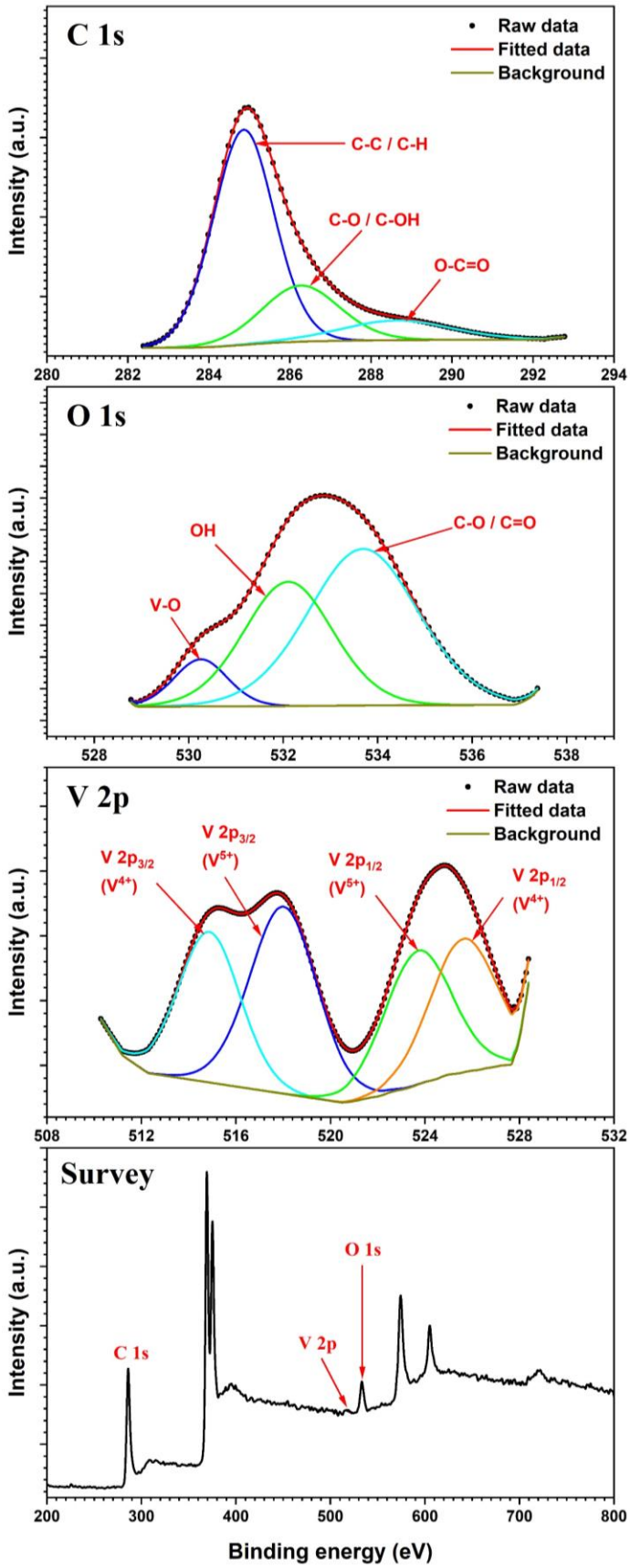

Fig .5: XPS survey and high-resolution spectra of the V 2p, O 1s, and C 1s core levels for vanadium oxide thin films deposited by RF magnetron sputtering.

The differences in surface chemistry, oxidation states, and contaminant levels between the films highlight the influence of plasma energy and ion bombardment associated with each deposition technique, where pulsed DC sputtering yields vanadium oxide films with more controlled stoichiometry and stable oxidation states, while RF sputtering produces more porous and reactive surfaces with higher oxidation, greater defect density, and enhanced adsorption of hydroxyl and carbon species.

3.4 FTIR analysis:

FTIR spectroscopy was employed to investigate the vibrational characteristics and chemical bonding states of vanadium oxide thin films deposited via pulsed DC and RF magnetron sputtering. The resulting spectra, presented in Fig. (6), reveal distinct absorption features that reflect the differences in phase composition and oxidation states arising from the two deposition techniques. These vibrational signatures show strong correlation with the structural and morphological findings obtained from XRD, SEM, and XPS analyses.

In the case of film deposited using pulsed DC magnetron sputtering, prominent absorption bands are observed at 459, 605, and 664 cm^{-1}, corresponding to V–O–V bending and stretching modes typically associated with mixed-valence vanadium oxides such as VO_2, V_6O_{13}, or V_2O_3 [52]. A sharp and well-defined band at 974 cm^{-1} is attributed to the terminal V=O (vanadyl) stretching vibration, indicative of VO_2-like bonding environments [52,53–55]. Furthermore, a band at 1110 cm^{-1}, associated with asymmetric V–O–V stretching, supports the presence of a distorted vanadium oxide framework. The higher wavenumber absorptions at 1887, 1988, 2094, and 2192 cm^{-1} likely represent overtone and combination bands involving O–H vibrations from surface hydroxyl groups and adsorbed water, and may also be linked to polymorphic VO_2 phases or mixed valence states involving V^{4+} and V^{5+} [52]. Their presence suggests a hydrated or hydroxylated surface, often linked to porous or disordered film structures. These FTIR features suggest limited oxidation during pulsed DC sputtering and reinforce the presence of oxygen-deficient phases, as supported by the film's characteristic blue coloration and the dominance of VO_2 signatures. These findings are consistent with XRD analysis, which revealed that pulsed DC-sputtered film is primarily composed of monoclinic VO_2, with partial contributions from orthorhombic V_2O_5 reflections [52,56]. The FTIR spectra further confirm this mixed-phase composition and the presence of reduced vanadium oxidation states. SEM micrographs complement these results by revealing a relatively thin, smooth, and dense film morphology with compact grains, which minimizes surface oxidation. This microstructural compactness aligns with the reduced presence of V^{5+} and supports the FTIR-detected VO_2-rich, sub-stoichiometric composition.

In contrast, the FTIR spectrum of the film deposited via RF magnetron sputtering exhibits a broader and more complex vibrational profile, indicative of a higher oxidation state and the formation of a more crystalline vanadium pentoxide (V_2O_5) structure. Prominent absorption bands observed at 473, 566, and 720 cm^{-1} are attributed to V–O–V stretching vibrations within the orthorhombic V_2O_5 lattice. The intense band at 1019 cm^{-1} corresponds to the terminal V=O stretching vibration, a definitive marker of well-ordered V_2O_5. Additional bands at 868 and 1097 cm^{-1} are associated with symmetric and asymmetric stretching modes of bridging oxygen atoms in polymeric V–O–V chains [57], further confirming the presence of a highly oxidized, V^{5+}-rich matrix. Moreover, the appearance of bands at 1247, 1340, and 1590 cm^{-1}, along with broader features at 1713, 1936, 2009, and 2063 cm^{-1}, suggests the presence of lattice distortions, combination bands, and possibly coordinated water molecules embedded within the crystalline framework [52,57]. The presence of these FTIR bands supports the XPS findings, which indicate that ambient air exposure during sample handling and transfer leads to the adsorption of surface-bound hydroxyl groups, water molecules, and organic contaminants. Collectively, these results confirm that even brief post-deposition exposure to ambient conditions can contribute to the O 1s and C 1s spectral features observed in XPS. These features are commonly observed in hydrated or structurally complex vanadium pentoxide networks, indicating an elevated degree of oxidation and structural complexity in the RF-sputtered films. The high porosity of the RF-deposited thin film, as observed through morphological analysis, likely contributes to greater exposure of the film surface to ambient oxygen. This facilitates the stabilization of fully oxidized V^{5+} states, favoring the formation of stoichiometric V_2O_5 rather than mixed-valence (V^{4+}/V^{5+}) configurations. Thus, the FTIR results corroborate the morphological and optical findings, highlighting the pronounced oxidation and crystallinity achieved via RF magnetron sputtering. These FTIR observations align well with XRD results, which show that RF-sputtered film contains a broader range of orthorhombic V_2O_5 reflections, along with less prominent VO_2 bands. The enhanced oxidation state and crystallinity inferred from FTIR are also supported by SEM analysis, which reveals a significantly thicker and porous nanostructure.

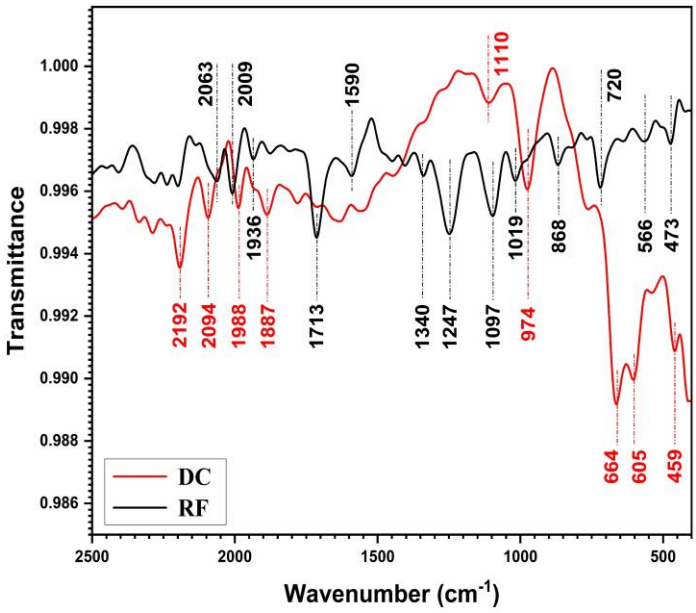

Fig. (6): FTIR Spectrum of vanadium oxide thin films deposited using pulsed DC magnetron sputtering and RF magnetron sputtering.

3.5 Electronic conductivity:

Figure (7) presents the current intensity–electric potential (I–V) characteristics of vanadium oxide thin films deposited via pulsed DC and RF magnetron sputtering. The corresponding values of resistance, electrical conductivity, and film thickness are summarized in Table (4). The electrical conductivity (σ_e) was calculated according to Equation (2):

$$\sigma_e = \left(\frac{1}{\rho}\right) = \left(\frac{L}{R.A}\right) \quad (2)$$

where **L** is the film thickness, **R** is the ohmic resistance, and **A** is the cross-sectional area of the thin film, which is equal to 1 cm^2 for both films. The electrical and structural characteristics of vanadium oxide thin films deposited via pulsed DC and RF magnetron sputtering exhibit significant performance differences, primarily influenced by the deposition method and resulting material properties. The I-V plots for both film types display linear behavior, indicating Ohmic conduction, wherein the current intensity is directly proportional to the applied electric potential [58,59]. This linearity confirms that charge transport is dominated by drift mechanisms rather than space-charge-limited conduction. Notably, the pulsed DC-deposited film exhibits a steeper I–V slope and a higher measured electrical conductivity of ~4.04 × 10^{-4} S/cm compared to ~3.22 × 10^{-4} S/cm for the RF-sputtered counterpart. Despite being slightly thinner (~350 nm vs. ~400 nm), the DC film demonstrates a lower resistance, indicative of more efficient charge transport pathways [59,60]. These enhanced electrical properties can be attributed to distinct structural and chemical differences between the films, as evidenced by XRD, SEM, XPS, and FTIR analyses. XRD patterns reveal that both films consist of mixed VO_2 and V_2O_5 phases; however, the DC-sputtered film contain a higher proportion of monoclinic VO_2, a phase known for its metal–insulator transition (MIT) near 68 °C and significantly higher electrical conductivity in the metallic state [61,62]. In contrast, the RF-deposited film is dominated by orthorhombic V_2O_5, a wide-bandgap semiconductor ($E_g \approx 2.2$–2.8 eV) with inherently lower electrical conductivity [61,62]. SEM micrographs further underscore these differences, with the pulsed DC film exhibiting a denser, more uniform grain structure and minimal porosity, leading to reduced grain boundary scattering and enhanced carrier mobility [63,64]. Conversely, RF film shows higher porosity and surface roughness, which increase carrier scattering and interrupt conduction pathways [58,59]. The morphological disparities are further reflected in the FTIR spectra. DC-deposited film displays vibrational modes associated with VO_2 and mixed V^{4+}/V^{5+} bonding, suggesting the presence of sub-stoichiometric phases that support electron hopping and delocalization. In contrast, RF-sputtered film exhibits strong V=O and V–O–V bands characteristic of fully oxidized V^{5+} in V_2O_5, which limits electrical conductivity [60,62]. Furthermore, pulsed DC sputtering tends to promote nanocrystalline growth, which has been linked to enhanced electronic transport [58,59]. The vanadium oxide thin films developed in this study exhibited superior electrical conductivity compared to values reported in earlier literature [35,65–67], highlighting the effectiveness of our optimized deposition conditions in improving charge transport. For instance, Margoni et al. [35] employed spray pyrolysis to fabricate V_2O_5 thin films and reported a maximum electrical conductivity of 1.0 × 10^{-5} $\Omega^{-1}.cm^{-1}$ at a substrate temperature of 375 °C. Similarly, Kovendhan et al. [65] achieved a conductivity of 1.5 × 10^{-6} $\Omega^{-1}.cm^{-1}$ for V_2O_5 films prepared via spray deposition. Sánchez et al. [66] synthesized bulk V_2O_5 using a melt-quenching process and reported a conductivity of 6.5 × 10^{-6} $\Omega^{-1}.cm^{-1}$. In another study, Chakrabarty et al. [67] examined polycrystalline V_2O_5 and found its conductivity to be 5 × 10^{-5} $\Omega^{-1}.cm^{-1}$.

In summary, the integration of I–V behavior with structural, morphological, and chemical data highlights the substantial impact of the sputtering technique on electronic transport in vanadium oxide films. Pulsed DC magnetron sputtering emerges as a superior deposition method for producing vanadium oxide thin films with enhanced electrical conductivity, optimized phase composition, and favorable microstructural attributes, making them well-suited for advanced applications such as smart windows, sensors, and electrochromic devices.

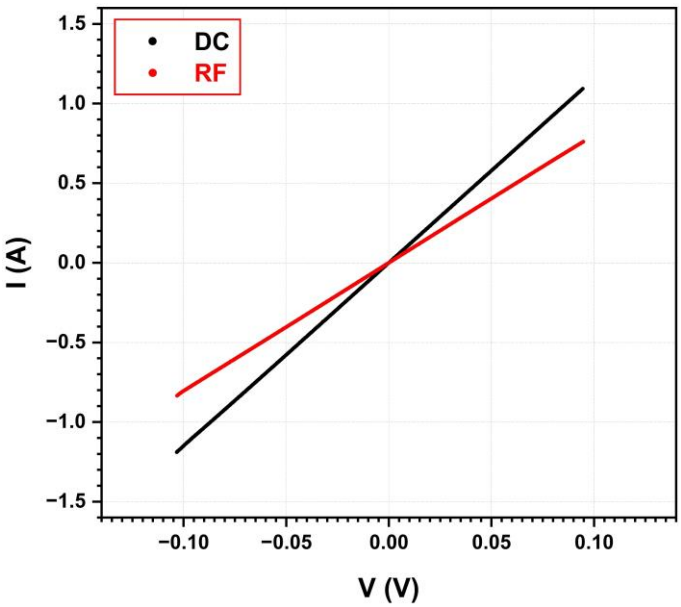

Fig. 7: Current intensity as a function of applied electric potential for vanadium oxide thin films deposited by pulsed DC magnetron sputtering and RF magnetron sputtering.

Table.4: Thickness, resistance, and electrical conductivity of vanadium oxide thin films deposited by pulsed DC magnetron sputtering and RF magnetron sputtering.

Deposition technique	Thickness (d, nm)	Resistance (R, Ω)	Electrical Conductivity (σ_e ×10^{-4} S/cm)
Pulsed DC	350 ± 10	0.0866 ± 9.98×10^{-6}	4.04 ± 1.15×10^{-5}
RF	400 ± 12	0.1242 ± 1.16×10^{-5}	3.22 ± 9.67×10^{-6}

4. Conclusion

This study clearly demonstrates that the choice of sputtering technique significantly affects the structural, morphological, and electrical properties of vanadium oxide thin films. Pulsed

DC magnetron sputtering resulted in VO_2-rich films characterized by compact morphology and superior electrical conductivity (~4.04×10^{-4} S/cm). In contrast, RF magnetron sputtering promoted the formation of V_2O_5-dominant films with a porous microstructure and lower conductivity (~3.22×10^{-4} S/cm). XRD analysis revealed a phase transition from monoclinic VO_2 to orthorhombic V_2O_5, accompanied by an increase in average crystallite size from ~10.12 nm (pulsed DC) to ~12.26 nm (RF). SEM analysis further indicated that pulsed DC film was smoother and denser, whereas RF-deposited film exhibited rougher surfaces. XPS confirmed distinct differences in vanadium oxidation states, lattice oxygen content, and surface contamination between the two deposition methods, underscoring the role of sputtering conditions in controlling surface chemistry and structural integrity. Complementary FTIR analysis identified vibrational modes corresponding to both VO_2 and V_2O_5, supporting the observed phase composition. Overall, these findings highlight the potential for tuning the properties of vanadium oxide thin films through controlled deposition parameters, offering valuable pathways for optimizing performance in electronic and energy-related applications.

CRediT authorship contribution statement:

All authors have made substantial contributions to this research. Conceptualization, F.M. and M.H.; methodology, A. A.; validation, F.M., M.H., and A.M.; formal analysis, A.A.; data curation, M.H. and A.A.; writing—original draft preparation, M.H. and A.A.; writing-review and editing, F.M. and A.M.; supervision, F.M. and A.M.; project administration, M.H.; funding acquisition, M.H. All authors have read and agreed to the published version of the manuscript.

Data availability statement

The data used to support the findings of this study are available from the corresponding author upon request.

Declaration of competing interest

The authors declare that they have no known competing financial interests or personal relationships that could have appeared to influence the work reported in this paper.

Acknowledgments

The authors gratefully acknowledge the financial support provided by the Science, Technology & Innovation Funding Authority (STDF) under grant number 46027. This funding was instrumental in facilitating the research and its outcomes.

References

[1] S. Tsunekawa, K. Asami, S. Ito, M. Yashima, T. Sugimoto, *Applied Surface Science*, 252 (2005) 1651–1656.

[2] F. Lin, X. Tong, Y. Wang, J. Bao, Z. M. Wang, *Nanoscale Research Letters*, 10 (2015) 435.

[3] A. V. Boris, Y. Matiks, E. Benckiser, A. Frano, P. Popovich, V. Hinkov, P. Wochner, M. Castro-Colin, E. Detemple, V. K. Malik, C. Bernhard, T. Prokscha, A. Suter, Z. Salman, E. Morenzoni, G. Cristiani, H.-U. Habermeier, B. Keimer, *Science*, 332 (2011) 937–940.

[4] S. Lee, I. N. Ivanov, J. K. Keum, H. N. Lee, *Scientific Reports*, 6 (2016) 19621.

[5] A. Srivastava, H. Rotella, S. Saha, B. Pal, G. Kalon, S. Mathew, M. Motapothula, M. Dykas, P. Yang, E. Okunishi, D. D. Sarma, T. Venkatesan, *APL Materials*, 3 (2015).

[6] Y.-B. Kang, *Journal of the European Ceramic Society*, 32 (2012) 3187–3198.

[7] F. J. Morin, *Physical Review Letters*, 3 (1959) 34–36.

[8] E. Strelcov, Y. Lilach, A. Kolmakov, *Nano Letters*, 9 (2009) 2322–2326.

[9] A. Crunteanu, J. Givernaud, J. Leroy, D. Mardivirin, C. Champeaux, J.-C. Orlianges, A. Catherinot, P. Blondy, *Science and Technology of Advanced Materials*, 11 (2010) 065002.

[10] S. Chen, Z. Wang, H. Ren, Y. Chen, W. Yan, C. Wang, B. Li, J. Jiang, C. Zou, *Science Advances*, 5 (2019) 764–772.

[11] R. Shi, X. Cai, W. Wang, J. Wang, D. Kong, N. Cai, P. Chen, P. He, Z. Wu, A. Amini, N. Wang, C. Cheng, *Advanced Functional Materials*, 29 (2019).

[12] R. Xie, C. T. Bui, B. Varghese, Q. Zhang, C. H. Sow, B. Li, J. T. L. Thong, *Advanced Functional Materials*, 21 (2011) 1602–1607.

[13] G. Savorianakis, K. Mita, T. Shimizu, S. Konstantinidis, M. Voué, B. Maes, *Journal of Applied Physics*, 129 (2021).

[14] G. Savorianakis, C. Rousseau, A. Sergievskaya, G. Rosolen, M. Voué, B. Maes, S. Konstantinidis, *Advanced Materials Interfaces*, 101 (2024).

[15] X. Chen, J. Dai, *Optik*, 121 (2010) 1529–1533.

[16] S. Vadnala, N. Paul, A. Agrawal, S. G. Singh, *Materials Science in Semiconductor Processing*, 81 (2018) 82–88.

[17] S. Wang, K. A. Owusu, L. Mai, Y. Ke, Y. Zhou, P. Hu, S. Magdassi, Y. Long, *Applied Energy*, 211 (2018) 200–217.

[18] J. Livage, *Materials*, 3 (2010) 4175–4195.

[19] Q. Su, C. K. Huang, Y. Wang, Y. C. Fan, B. A. Lu, W. Lan, Y. Y. Wang, X. Q. Liu, *Journal of Alloys and Compounds*, 475 (2009) 518–523.

[20] T. W. Chiu, K. Tonooka, N. Kikuchi, *Thin Solid Films*, 518 (2010) 7441–7444.

[21] K. V. Madhuri, B. S. Naidu, O. M. Hussain, M. Eddrief, C. Julien, *Materials Science and Engineering: B*, 86 (2001) 165–171.

[22] L. Chotirat, S. Niyomwas, W. Wongpisan, S. Supothina, *Journal of Nanotechnology*, 2021 (2021) 1–7.

[23] G. Li, S. Pang, L. Jiang, Z. Guo, Z. Zhang, *Journal of Physical Chemistry B*, 110 (2006) 9383–9386.

[24] M. S. B. De Castro, C. L. Ferreira, R. R. De Avillez, *Infrared Physics and Technology*, 60 (2013) 103–107.

[25] X.-Q. Zhao, H.-D. Zhou, J.-M. Chen, *Materials Science and Engineering: A*, 431 (2006) 290–297.

[26] B. Uzakbaiuly, A. Mukanova, Y. Zhang, Z. Bakenov, *Frontiers in Energy Research*, 9 (2021).

[27] M. Becker, J. Kessler, F. Kuhl, S. L. Benz, L. Chen, A. Polity, P. J. Klar, S. Chatterjee, *physica status solidi (a)*, 219 (2022).

[28] K. Gupta, S. Kumar, R. Singhal, *International Journal of Recent Technology and Engineering (IJRTE)*, 8 (2019) 7899–7902.

[29] M. Zhu, D. Zhang, S. Jiang, S. Liu, H. Qi, Y. Yang, *Ceramics International*, 47 (2021) 15491–15499.

[30] R. Plugaru, I. Mihalache, C. Romaniţan, F. Comanescu, S. Vulpe, G. Craciun, N. Plugaru, N. Djourelov, *Sensors*, 23 (2023) 1759.

[31] E. Ekström, S. Hurand, M. M. Yildizhan, A. Elsukova, P. O. Å. Persson, B. Paul, G. Ramanath, A. le Febvrier, F. Eriksson, P. Eklund, *Advanced Physics Research*, 2 (2023).

[32] P. Scherrer, *Nachrichten von der Gesellschaft der Wissenschaften zu Göttingen, Mathematisch-Physikalische Klasse*, 1918 (1918) 98–100.

[33] Z. Zeng, W. Liang, H. Liao, H. L. Xin, Y. Chu, H. Zheng, *Nano Letters*, 14 (2014) 1745–1750.

[34] F. M. Ross, *Science*, 350 (2015) aaa9886(1-9).

[35] M. M. Margoni, S. Mathuri, K. Ramamurthi, R. R. Babu, K. Sethuraman, *Applied Surface Science*, 418 (2017) 280–290.

[36] Z. Luo, X. Zhou, D. Yan, D. Wang, Z. Li, C. Yang, Y. Jiang, *Thin Solid Films*, 550 (2014) 227–232.

[37] A. Kumar, P. Singh, N. Kulkarni, D. Kaur, *Thin Solid Films*, 516 (2008) 912–918.

[38] J. Scarminio, P. R. C. da Silva, R. V. Gelamo, M. A. B. de Moraes, *Matéria (Rio de Janeiro)*, 22 (2017).

[39] A. Dey, M. K. Nayak, A. C. M. Esther, M. S. Pradeepkumar, D. Porwal, A. K. Gupta, P. Bera, H. C. Barshilia, A. K. Mukhopadhyay, A. K. Pandey, K. Khan, M. Bhattacharya, D. R. Kumar, N. Sridhara, A. K. Sharma, *Scientific Reports*, 6 (2016) 36811.

[40] W. Somkhunthot, N. Pimpabute, T. Seetawan, *Materials Sciences and Applications*, 03 (2012) 645–649.

[41] A. Garcia-Valenzuela, C. Lopez-Santos, R. Alvarez, V. Rico, J. Cotrino, A. R. Gonzalez-Elipe, A. Palmero, *Nanotechnology*, 28 (2017) 465605.

[42] C. Batista, J. Mendes, V. Teixeira, J. Carneiro, *Materials Science Forum*, 587–588 (2008) 343–347.

[43] S. M. Kozlowski, The Effect of Substrate Bias on the Growth of Vanadium Oxide Thin, The Pennsylvania State University, The Graduate School, (2014) 79.

[44] C. M. Julien, A. Mauger, O. M. Hussain, *Materials*, 12 (2019) 2687.

[45] G. Silversmit, D. Depla, H. Poelman, G. B. Marin, R. De Gryse, *Journal of Electron Spectroscopy and Related Phenomena*, 135 (2004) 167–175.

[46] E. Cazzanelli, G. Mariotto, S. Passerini, W. H. Smyrl, A. Gorenstein, *Solar Energy Materials and Solar Cells*, 56 (1999) 249–258.

[47] Y. Wu, L. Fan, W. Huang, S. Chen, S. Chen, F. Chen, C. Zou, Z. Wu, *Physical Chemistry Chemical Physics*, 16 (2014) 17705.

[48] D. Goodacre, M. Blum, C. Buechner, H. Hoek, S. M. Gericke, V. Jovic, J. B. Franklin, S. Kittiwatanakul, T. Söhnel, H. Bluhm, K. E. Smith, *The Journal of Chemical Physics*, 152 (2020).

[49] G. Greczynski, L. Hultman, *Vacuum*, 205 (2022) 111463.

[50] G. Greczynski, L. Hultman, *ChemPhysChem*, 18 (2017) 1507–1512.

[51] G. Greczynski, S. Mráz, L. Hultman, J. M. Schneider, *Applied Surface Science*, 385 (2016) 356–359.

[52] B. F. Hassan, M. J. Dathan, A. A. Abdallah, *Iraqi Journal of Science*, (2021) 3536–3544.

[53] L. D. Frederickson, D. M. Hausen, *Analytical Chemistry*, 35 (1963) 818–827.

[54] M. H. Ismail, A. H. Ali, S. M. Thahab, *Characterization and Application of Nanomaterials*, 6 (2024) 3665.

[55] X. Chen, P. Wang, Z. Feng, Y. Liu, M. Cui, C. Meng, Y. Zhang, *Advanced Sensor and Energy Materials*, 1 (2022) 100013.

[56] G. Ekinci, B. Özkal, N. A. A. S. Al-Jawfi, S. Kazan, *Journal of Advanced Applied Sciences*, 2 (2023) 57–63.

[57] S. Nagasundar, A. A. Kaliani, S. Subin, S. Ayyasamy, *Oriental Journal Of Chemistry*, 41 (2025) 111–119.

[58] H. A. Basantani, Effect of Rf Substrate Bias on Vanadium Oxide Thin Films During Reactive Pulsed DC Magnetron Sputter Deposition, Pennsylvania State University, 2011.

[59] N. Fieldhouse, S. M. Pursel, R. Carey, M. W. Horn, S. S. N. Bharadwaja, *Journal of Vacuum Science & Technology A: Vacuum, Surfaces, and Films*, 27 (2009) 951–955.

[60] V.H. Lam, Electrical Properties Of Reactive Magnetron Sputtered Vanadium Oxide Thin FilmsOxide Thin Films, University of Central Florida Libraries, 2006.

[61] A. Christensen, A. B. Posadas, B. Zutter, P. Finnegan, S. Bhullar, S. Bishop, A. A. Talin, A. A. Demkov, *Journal of Applied Physics*, 134 (2023) 1–19.

[62] B. Akyürek, Electrical Characterization of Vanadium (VO_2) Thin Films Grown by Magnetron Sputtering Technique, İzmir Institute of Technology, 2024.

[63] J. T. Gudmundsson, N. Brenning, D. Lundin, U. Helmersson, *Journal of Vacuum Science & Technology A: Vacuum, Surfaces, and Films*, 30 (2012).

[64] E. H. Sondheimer, *Advances in Physics*, 50 (2001) 499–537.

[65] M. Kovendhan, D. Paul Joseph, P. Manimuthu, A. Sendilkumar, S. N. Karthick, S. Sambasivam, K. Vijayarangamuthu, H. J. Kim, B. C. Choi, K. Asokan, C. Venkateswaran, R. Mohan, *Current Applied Physics*, 15 (2015) 622–631.

[66] C. Sanchez, R. Morineau, J. Livage, *Physica Status Solidi (a)*, 76 (1983) 661–666.

[67] D. K. Chakrabarty, D. Guha, A. B. Biswas, *Journal of Materials Science*, 11 (1976) 1347–1353.